East Asian monsoon intensification promoted weathering of the magnesium-rich southern China upper crust and its global significance

Yibo Yang, Albert Galy, Xiaomin Fang, Christian France-Lanord, Shiming Wan, Rongsheng Yang, Jian Zhang, Ran Zhang, Song Yang, Yunfa Miao, et al.

Cenozoic advance of the East Asian monsoon promoted carbon dioxide consumption by weathering of the Mg-rich southern China upper crust

Yibo Yang[1, 2*], Albert Galy[3], Xiaomin Fang[1, 2, 4*], Christian France-Lanord[3], Shimming Wan[5, 6], Rongsheng Yang[1, 3], Jian Zhang[1], Ran Zhang[7], Song Yang[8], Yunfa Miao[9], Chengcheng Ye[1], Yudong Liu[1, 4]

[1]Key Laboratory of Continental Collision and Plateau Uplift, Institute of Tibetan Plateau Research, Chinese Academy of Sciences, Beijing 100101, China
[2]CAS Center for Excellence in Tibetan Plateau Earth Sciences, Beijing 100101, China
[3]Centre de Recherches Pétrographiques et Géochimiques, UMR7358, CNRS - Université de Lorraine, 54500 Vandoeuvre les Nancy, France
[4] University of Chinese Academy of Sciences, Beijing 100049, China
[5]Key Laboratory of Marine Geology and Environment, Institute of Oceanology, Chinese Academy of Sciences, Qingdao 266071, China
[6]Function Laboratory for Marine Geology, National Oceanography Laboratory, Qingdao 266061, China
[7]Climate Change Research Center, Institute of Atmospheric Physics, Chinese Academy of Sciences, Beijing 100029, China
[8]Key Laboratory of Tibetan Environment Changes and Land Surface Processes, Institute of Tibetan Plateau Research, Chinese Academy of Sciences, Beijing 100101, China
[9]Key Laboratory of Desert and Desertification, Northwest institute of Eco-Environment and Resources, Chinese Academy of Sciences, Lanzhou,730000, China
*Corresponding authors: yangyibo@itpcas.ac.cn (Y. Yang) or fangxm@itpcas.ac.cn (X. Fang)

Abstract

The Oligocene-Miocene boundary climatic reorganization linked to the northward advance of the East Asian monsoon in subtropical China is a potentially important but poorly constrained atmospheric CO_2 sink. Here, we performed a first-order estimate of the difference in CO_2 consumption induced by silicate chemical weathering and organic carbon burial in subtropical China related to this monsoon advance. The results highlight the significant role of weathering of the Mg-rich upper continental crust in East China that would contribute significantly to the rise in the Mg content of

the ocean during the Neogene. Our results show that an increase in CO_2 consumption by silicate weathering varies between ~1% and 15% of the current global continental silicate sink with an ~60% contribution of Mg-silicate weathering since the late Oligocene but a negligible increase in the global organic carbon burial (<3.5%). The carbon impact of the northward advance of the East Asian monsoon is therefore significant but strongly related to the Mg-rich nature of the crust affected by such climatic change. Further modelling work indicates that the uplift of the northern Tibetan Plateau plays a key role in this monsoon advance. Our study thus suggests that the uplift of the Himalayas-Tibetan Plateau can lead to indirect modification of the carbon cycle and the global climate by changing the regional hydrological cycle in areas of East Asia that are tectonically inactive in addition to the direct impact of high erosion and organic carbon burial along the orogenic belt in South Asia.
Keywords: Tibetan Plateau; Late Oligocene; silicate weathering; carbon cycle; oceanic Mg cycle

1. Introduction

Atmospheric CO_2 consumption by silicate weathering and organic carbon burial are the sinks that control atmospheric CO_2 levels over geological timescales. Complex feedback mechanisms between climate and tectonics led to a hypothesis that the uplift of the Himalayas-Tibetan Plateau (TP) was a primary driver of Cenozoic atmospheric CO_2 decline and global cooling predominantly through accelerating silicate chemical weathering in the India-Asia collision zone (Raymo and Ruddiman et al., 1992; Kump et al., 2000), while debated (e.g., Blum et al., 1998), and through effective burial of organic carbon in the nearby Bengal Fan in South Asia (France-Lanord and Derry, 1997; Galy et al., 2007; Lee et al., 2019). However, orogenic uplift also contributed to the increase in monsoonal rainfall by the expansion of the East Asian monsoon and, as such, might have extensive control over the geological carbon cycle by enhancing silicate chemical weathering and/or burial of organic carbon in East Asia, namely, outside the Bay of Bengal (Fig. 1).

The modern East Asian climatic pattern is likely to have been established at the Oligocene-Miocene boundary with an arid zone restricted to Northwest China, in contrast to a relatively broad belt of aridity stretching across China from west to the east during the Palaeogene (Fig. 1, Guo et al., 2008; Sun and Wang, 2005;). The onset of the East Asian monsoon was recently proposed to be during the Eocene, but monsoonal activities were restricted to regions not exceeding the far south of China

(e.g., Licht et al., 2014; Spicer et al., 2016; Xie et al., 2020). Monsoon penetration into modern arid Northwest China may have extensively occurred only from the latest early Oligocene to early Miocene, as suggested by fossil evidence (Guo et al., 2008; Miao et al., 2013; Song et al., 2019; Sun and Wang, 2005). This reorganization of the climate system around the Oligocene-Miocene boundary from arid to modern, monsoon-like humid in this broad region involves a total area of ~ 3.2×10^6 km^2 (Fig. 1). The increase in rainfall due to the monsoon advance over such a broad region is thus expected to not only enhance silicate weathering but also accelerate terrestrial organic carbon production. In particular, weathering of Mg-enriched Yangtze and North China cratons in East China (Gao et al., 1991, 1998), which makes up the majority of the area affected by climatic reorganization around the Oligocene-Miocene boundary (Fig. 1b), could yield a more significant atmospheric CO_2 sink than the weathering of Mg-depleted Himalayan terranes (e.g., France-Lanord and Derry, 1997). To test this hypothesis, we performed a first-order estimate of the changes in CO_2 consumption flux from silicate weathering and organic carbon burial through the Palaeogene-Neogene boundary using the chemistry of sediments in the South China Sea (SCS) and soils in East China regions.

2. Material and methods

2.1 Quantifying carbon dioxide consumption by silicate weathering

Quantification of the release of soil base cations in silicate weathering can be done only by normalizing their abundances to that of an immobile element, and we used Al since other immobile elements, such as Ti, are more sensitive to changes in the composition of the regolith (e.g., Ti is relatively enriched in mafic rocks in the upper crust of eastern China, Gao et al., 1991). Given that Al is an immobile element during bedrock weathering, the CO_2 consumption ($mol \cdot kg^{-1}$) due to weathering of silicates in bedrock for a given base cation (ΔX_0) can be estimated by:

$$\Delta X_0=([X]_{bedrock}-[Al]_{bedrock}/[Al]_{soil}\times[X]_{soil})/M_X\times100 \quad (1),$$

where [X] shows the concentration (%) of element X measured in soil and bedrock and M is the molar mass for a given element X. The overall CO_2 consumption on geological timescales (>1 Myr) by silicate weathering (C_{sil}) between bedrock and soil can thus be estimated by the overall difference of soil base cations:

$$C_{sil} = \Delta Ca_0+\Delta Mg_0+0.10\Delta K_0+0.15\Delta Na_0 \quad (2),$$

assuming that all the alkalinity equivalent to Mg^{2+} and Ca^{2+} lost from silicate minerals ultimately precipitates as marine carbonate, that only a fraction of the alkalinity is associated with alkalis (20% for K^+ and 30% for Na^+) and that there is no “reverse

weathering" as a sink for these base cations in marine settings (France-Lanord and Derry, 1997).

The change in CO_2 consumption by silicate weathering (Δ_{sil}) can be evaluated by chemical differences between the soil in the study area after and before climatic reorganization. Then, the overall difference in average soil base cations between arid loess and humid red soils (Δ_{sil}) can be estimated as:

$$\Delta_{sil} = C_{sil,\,a} - C_{sil,\,b}$$
$$= (\Delta Ca_{0,\,a} - \Delta Ca_{0,\,b}) + (\Delta Mg_{0,\,a} - \Delta Mg_{0,\,b}) + 0.10\,(\Delta K_{0,\,a} - \Delta K_{0,\,b}) + 0.15\,(\Delta Na_{0,\,a} - \Delta Na_{0,\,b})$$
$$= \Delta Ca + \Delta Mg + 0.10\Delta K + 0.15\Delta Na \quad (3),$$

where subscripts "b" and "a" denote after and before the monsoon advance, respectively.

Because the tectonic setting in East China involving the assembly of the North China craton, Qinling Orogen and Yangtze craton formed prior to the Cenozoic (Zheng et al., 2013), we assumed that bedrock in East China exhibits the same composition between the Paleogene and the Neogene. Palaeogene arid soil composition is difficult to estimate due to the lack of data. However, a modern analogue of soil under semi-arid and arid settings could be the widespread eolian loess in northern China, which is typical of the well-mixed upper continental curst and is subject to only weak chemical weathering under arid climates (e.g., Gallet et al., 1996). Due to loess compositional homogeneity, we used the Xifeng (XF) Pleistocene loess (Fig. 1, Table S1) from northern China to represent lithosols and cambisols distributed in the modern arid/semi-arid climate (Fig. 2a). Loess can bear carbonates, but its composition after acetic acid leaching could be typical of soil silicate compositions in Palaeogene arid climates. However, loess, lithosols and cambisols from NW China might not have been formed from the same regolith as the weathered crust of southern East China. Thus, the estimates of related terms, e.g., C_{sil} and Δ_{sil}, could be biased. Such provenance bias is negligible except for ΔMg due to regional heterogeneity of Mg-bearing minerals in the upper crust rocks and the peculiar occurrence of a Mg-rich upper crust in East China (Gao et al., 1991, Gao et al., 1998).

Typical soils in humid subtropical China related to late Oligocene climatic reorganization are red earth and yellow earth, which account for ~80% of red soils in China (He et al., 2004). Red and yellow earths are similar in composition but different in colour, as they contain different iron oxides (hematite and goethite, respectively). Here, we chose the average compositions of four red earth datasets and three yellow earth datasets that are well spaced and can represent widespread acrisols in subtropical China (Fig. 2a; Table S1). The red earth datasets included Quaternary red earth compositions along the Yangtze River (Dongting Lake, DTL, a regional

investigation of red soils covering 1.4×10^4 km^2, Zhang et al., 2007; Jiujiang, JJ, a 10.4 m thick red earth profile, and Xuancheng, XC, a 14 m thick red earth profile, Hong et al., 2013) and a red earth average across the entire South China (77 data of A horizon of soil profiles; CNEMC, 1990). The yellow earth datasets included Quaternary typical yellow earth compositions (Nanxiong, NX, a 2.4 m thick yellow earth profile; Tianyang, TY, a 4.2 m thick yellow earth profile) around the southern boundary of the subtropical zone (Table S1) and a yellow earth average across the entire South China (37 data of A horizon of soil profiles across South China, CNEMC, 1990). Gleysols from the lower reaches of the Yangtze and Yellow Rivers were not considered here because they are cultivated soils.

In our study, the NX and TY yellow earth samples were oven-dried, ground into powder, and leached by diluted acetic acid. Diluted acetic acid leaching will introduce few Ca from silicates. The residues were digested by pressurized acid digestion using a mixture of HNO_3/HF. Major elements were analysed by inductively coupled plasma optical emission spectroscopy (ICP-OES, Leeman Labs Prodigy-H) at the Institute of Tibet Plateau Research, Chinese Academy of Sciences. Concentrations of all elements were normalized to the weight of the bulk leached residues. Replicate analyses of samples showed relative standard deviations of <2%. Except NX and TY yellow earth samples with acetic leaching residues, other data used here are whole rock data. Since few amounts of carbonates exist in such low-pH environments in south China, the two types of data are comparable.

To impart constraints on changes in soil silicate composition in response to global cooling and regional climate variability during the Neogene, we also estimated Δ_{sil} variability using the average compositions of diluted acetic acid leached sediments of Ocean Drilling Program (ODP) site 1146 in the SCS (Fig. 1a). These sediments represent an average of the eroded silicates from southern East China (e.g., Liu et al. 2003). Considering the variation in silicate weathering intensity, two stages have been defined at 15-19 Ma (SCS 15-19 Ma) and 0-5 Ma (SCS 0-5 Ma), corresponding to strong and weak silicate weathering intensity stages, respectively (Wan et al., 2010). We used these two stages as the Neogene composition and, similar to our soil approach, compared it to the arid loess in North China.

2.2 Quantifying carbon dioxide consumption by organic carbon burial

Changes in the organic carbon burial (Δ_{oc}) after and before climatic reorganization can be quantified by measuring the difference in the terrestrial organic carbon content in East and South Asia clastic sediments. However, Δ_{oc} cannot be

directly evaluated using data from marginal sea sediments because it is difficult to distinguish terrestrial and marine contributions to bulk organic carbon. When Δ_{oc} was directly evaluated using marginal sea sediments, a dominance of marine organic material was revealed (Shipboard Scientific Party, 2000). However, by analogy with the findings in the Bay of Bengal (e.g., Galy et al., 2007; Lee et al. 2019), we assumed that Δ_{oc} is principally controlled by terrestrial organic carbon production and burial efficiency in marine sediments, and Δ_{oc} could be simply estimated as:

$$\Delta_{oc} = M_a \times f_a - M_b \times f_b \quad (4),$$

where M denotes organic matter content in soils, f denotes the organic carbon burial efficiency (percentage of organic carbon preserved in sediments), and the subscripts "a" and "b" denote after and before the monsoon advance, respectively.

2.3. Quantifying monsoon rainfall in response to tectonic uplift

To further constrain the orogenic uplift effect on the precipitation change in monsoon-influenced region in East China, we used a climate model to test precipitation differences between the modern topography and Palaeogene topography. Boundary conditions of the model corresponded to a change in topography only in the northern part of the TP since 1) uplift of this region exhibited a profound impact on the East Asian monsoon (Liu et al., 2015) and 2) the major uplift-related topographic change in this region occurred over the Neogene (e.g., Tapponnier et al., 2001; Lin et al., 2020). Two experiments were conducted with different topographies. The first utilized modern conditions with the present topography. In the second experiment, the northern TP was removed according to the uplift history of the TP (Tapponnier et al., 2001), which represents the Oligocene condition. Thus, the difference between the experiments gives the climatic effects of the rise of the northern part of the TP.

We employed the Community Earth System Model version 1.2.2 (CESM1.2.2) developed by the National Center of Atmospheric Research (NCAR). This model consists of atmosphere, ocean, land, river runoff, sea ice, land ice, and ocean wave components that interact with each other through a coupler. However, only the first 5 components were active in the model used in this study (see details in Zhang et al., 2019). Both experiments are run with a CO_2 concentration of 560 ppmv, which is higher than the present concentration and represents the late Oligocene level based on various proxies (Beerling and Royer, 2011). The concentrations of chloro-fluoro-carbon (CFCs) were set to 0, and those of CH_4 and N_2O were set 760 ppbv and 270 ppbv, respectively. All the other conditions, including O3 and aerosol concentrations, the solar constant and orbital parameters, were set to preindustrial

conditions. Both experiments were run for 1700 model years, which is long enough for the atmosphere and ocean surface layer to reach quasi-equilibrium. The last 50 years of data from each experiment were analysed and presented in this study.

3 The magnitude of silicate weathering and organic carbon burial change

3.1 Silicate alteration and Mg contribution

The results of C_{sil} show a high contribution of Ca-bearing mineral weathering (ΔCa_0) in all chosen weathered products in humid subtropical China and arid northern China but a distinct pattern of Mg contribution (ΔMg_0) between the two regions (Fig. 3a). C_{sil}^*, defined as $C_{sil}^*=C_{sil}-\Delta Mg_0$, could be used to account for CO_2 consumption by the chemical weathering of Ca-Na-K silicate minerals only (mainly feldspar). There are significant differences between C_{sil}^* and C_{sil} for the SCS sediments, the yellow and red earths, but there are few differences for the XF loess. This contrast suggests a dominant climate-induced weathering behaviour that is characterized by a greater depletion of Mg and Ca in humid subtropical China than in arid northern China. This climate-induced weathering contrast can also be supported by the results of Δ_{sil} that can be regarded as the composition difference of weathering products between intense and weak weathering regimes (Fig. 3b). The detail of the contribution from each cation shows decreasing CO_2 consumption values with $\Delta Mg>\Delta Ca>\Delta Na>\Delta K$ (Fig. 3b, Table S2), in line with the relative mineral stability during weathering (e.g., Mg-bearing minerals weather the fastest, followed by Ca-feldspar, Na-feldspar, and finally K-feldspar). Furthermore, the Δ_{sil}/C_{sil} ratios yield a mean of ~50% for SCS sediments and ~60% subtropical soils, suggesting a dominant cation yield by intense weathering in humid South China.

The Δ_{sil} pattern is suitable for displaying silicate alteration related to late Oligocene monsoon advance. Similarly, Δ_{sil}^*, defined as $\Delta_{sil}^*=\Delta_{sil}-\Delta Mg$, was used to account for CO_2 consumption by the chemical weathering of Ca-Na-K silicate minerals only (mainly feldspar). The difference between Δ_{sil} and Δ_{sil}^* indicates that the relative contribution of ΔMg is always >60% (Table S3). Δ_{sil}^* ranged from 0.12 to 0.16 $mol \cdot kg^{-1}$ for SCS sediments and from 0.18 to 0.22 $mol \cdot kg^{-1}$ for modern soils (Fig. 3b). Differences for the SCS sediments (19-15 Ma vs. 5-0 Ma) regarding different silicate weathering intensities (Table S3) suggest that the variability of Neogene climate/provenance for Δ_{sil*} and Δ_{sil} is probably within 20-30%. These Δ_{sil}^* values are comparable to CO_2 consumption by silicate weathering in ODP 116 sediments in the Bengal Fan (Fig. 1), where CO_2 consumption (C_{sil}) is between 0.17 $mol \cdot kg^{-1}$ for illite-chlorite sediments with no contribution from ΔMg and 0.23 $mol \cdot kg^{-1}$ for

smectite-kaolinite sediments with a contribution of only ~ 0.03 mol·kg^{-1} by ΔMg (Fig. 3a; France-Lanord and Derry, 1997). This suggests a comparable magnitude of CO_2 consumption by silicate alteration except for Mg for both regions.

Overall, the key difference in monsoon-influenced silicate weathering in subtropical China is the dominant effect of weathering of Mg-bearing silicates, which is likely related to the higher Mg concentrations in the Yangtze and Northern China cratons (e.g., Gao et al., 1991; Gao et al., 1998) than in the average upper continental crust (UCC, e.g., Rudnick and Gao, 2014) or the Himalayan crust (e.g., France-Lanord and Derry, 1997). For example, the relatively low ΔMg contribution < ~ 0.03 mol·kg^{-1} in South Asia corresponds to High Himalayan crystalline rocks with low MgO (1.76%, France-Lanord and Derry, 1997). Further, the erosional products have higher MgO contents (with a mean of 3.12%, n=30) for the fine-grained silicate sediments in the Yangtze River (He et al., 2015) than those in the XF loess (2.76%) (Table S1). These observations conform to that East China (carbonate-free composition), compared with other terranes (e.g., the Canadian shield), contains large proportions of unmetamorphosed supracrustal units that are considered to have, on average, higher proportions of mafic volcanics (Gao et al., 1998; Rudnick and Gao, 2004). Generally, the high ΔMg contribution can result from the facts that 1) Mg-rich upper crust rocks will be strongly depleted during soil silicate weathering and 2) the upper crust that experienced the intensification of climate-induced weathering is a Mg-rich portion. Such low MgO content preserved in red and yellow earths under a humid climate (Fig. 1) that dominated the Mg-rich upper crust in East China thus suggests a significantly higher Mg loss by weathering of the East China upper crust affected by late Oligocene climatic reorganization.

3.2 Organic carbon burial

To estimate $\Delta_{oc,}$ we first qualified the organic carbon burial efficiency, *f*. It is suggested that a high *f* value mainly results from high erosion/rapid deposition systems (Blair and Aller, 2012), e.g., the Bengal Fan (Galy et al., 2007) and steep mountain rivers (Hilton et al., 2011). The Neogene monsoon climate in subtropical China can generate a large delivery of suspended sediments to the ocean in comparison with that in the Palaeogene (e.g., Métivier et al., 1999; Clift et al., 2004). Since the Yangtze River is the major carrier of sediments in subtropical China, we conservatively assumed that both f_a and f_b were ~30%, the *f* value for the modern Yangtze River (Blair and Aller, 2012), which yielded a minimum estimation of $\Delta_{oc.}$

The modern soil organic carbon content is 0.8-1.8% in most subtropical China

and is 0.4-0.8% in arid-semi-arid China for surface soil horizons (0 to 30 cm) (Fig. 2b). The area-weighted mean values are 1.3±0.6% (excluding cultivated soils in East China) and 0.7±0.3% for humid subtropical China and arid North China, respectively. Given a mean of ~0.2% for the fossil carbon content inherited from parent rock in SE Asia (France-Lanord and Derry, 1997; Hilton et al, 2011) and assuming its burial efficiency of 100%, M_a and M_b were assumed to be 0.89 and 0.39 mol·kg^{-1}, respectively, and together yielded a Δ_{oc} of 0.15 mol C·kg^{-1}. This Δ_{oc} is less than Δ_{sil}, exhibiting a mean value of 0.60 mol·kg^{-1} in subtropical China, which contrasts with the Himalayas, where the Δ_{oc} is much larger than Δ_{sil} (France-Lanord and Derry, 1997).

4. Discussion

4.1 Erosion rate related to the late Oligocene monsoon advance

Assessing the role of monsoon advance-induced silicate weathering and organic carbon burial in the context of the global budget requires an historical estimation of the volume of the crust subjected to erosion. We reconstructed this temporal variation in erosion flux as described in the following paragraphs.

In modern settings, the physical erosion of subtropical China is highly variable with ^{10}Be-based erosion rates from 20-50 mm·kyr^{-1} in low relief areas to 700-900 mm·kyr^{-1} in steep, landslide-dominated mountain terrane (Chappel et al., 2006). The drainage basin of the Yangtze River is mainly located within the study area (Fig. 1a) and accounts for 59% of the study area. In addition, the Yangtze River drains variable landscapes and climates and is thus likely to provide an area-averaged erosion rate for the whole studied area. Therefore, we assumed that the physical erosion of subtropical China (total area of ~ 3.2 × 10^6 km^2) is ~800×10^6 t·yr^{-1} by extrapolation of 480×10^6 t·yr^{-1} for the Yangtze River (Milliman and Syvitski, 1992).

We then assumed that the long-term variations in erosion flux related to subtropical China could generally scale with the temporal variations in the sediment budget around the East China marginal basins. The existing Cenozoic sediment budgets for the major basin systems of East Asia have yielded distinct long-term variations (Clift, 2004; Métivier et al., 1999). The results of Clift et al. (2004) including the Pearl River, East China Sea and Bohai Bay display different long-term variations with peaks of sedimentation in the Mid-Miocene and Quaternary (Clift et al., 2004; Fig. 4a). Métivier et al. (1999) showed a monotonous increase in the sedimentation rate in the East China Platform, which includes the East China Sea/North Taiwan, Okinawa, Yellow Sea and Bohai Bay (Fig. 4a). Clarification of

both variations is out of the aim and scope of this study; thus, we used our modern estimate of erosion flux to multiply the two relative variations of sediment discharges to construct two records of erosion flux related to subtropical China climatic reorganization since the late Oligocene (Fig. 4a).

4.2 Mg flux linked to the monsoon advance

The Mg flux variation linked to the monsoon advance from silicate weathering, $F_{Mg,\ sil}$, can be calculated as follows:

$$F_{Mg,\ sil} = E_a \times \Delta Mg_{0,\ a} - E_b \times \Delta Mg_{0,\ b} \quad (5),$$

where E is sediment yield ($kg \cdot yr^{-1}$) and it corresponds to our reconstructed erosion flux (Figs. 4a). $\Delta Mg_{0,\ b}$ is 0.03 $mol \cdot kg^{-1}$, identical to XF loess (Fig. 3a). 0.45 $mol \cdot kg^{-1}$ for $\Delta Mg_{0,\ b}$ is the mean of ΔMg_0 for SCS sediments and red soils in subtropical China (Fig. 3).

In addition, the sedimentary cover of East China bears a significant amount of dolostone lithology (e.g., Gao et al., 1991). The Neogene intensification of the weathering of that area would also have dissolved a relatively large amount of Mg-rich carbonate, further delivering Mg to the oceanic cycle. The Mg and Ca concentrations related to carbonate in the eastern China upper crust can be estimated by the comparison of the CEC upper crust compositions with and without carbonate (Gao et al., 1998). Assuming Si resides in only silicates, then the Mg molar concentration in carbonate ($[Mg]_{carb}$, $mol \cdot kg^{-1}$) can be estimated as follows:

$$[Mg]_{carb} = [Mg]_{bulk} - [Mg]_{sil}/[Si]_{bulk} \times [Si]_{sil} \quad (6),$$

where the subscripts “bulk” and “sil” denote element molar concentrations the CEC upper crust compositions with and without carbonates, respectively. The estimated $[Mg]_{carb}$ is 0.37 $mol \cdot kg^{-1}$, and $[Ca]_{carb}$ is 0.80 $mol \cdot kg^{-1}$, as calculated by the same approach. The molar Mg/Ca ratio in carbonate in eastern China is 0.46, which indicates that approximately 50% of carbonate minerals are dolomite, given a molar Mg/Ca ratio of 0.08 for calcite (a lower limit of average post-Archean carbonates in East China, Gao et al., 1991) and a molar Mg/Ca ratio of 1 for dolomite, supporting the above observation of a dolostone-rich lithology in East China. Since dolomite is hard to dissolve in arid and semi-arid settings (e.g., in arid NW China), we assumed that only calcite dissolves in arid settings before the monsoon advance and that both calcite and dolomite dissolve in humid settings after the monsoon advance. The Mg flux variation linked to the monsoon advance through carbonate weathering, $F_{Mg,\ sil}$, can be calculated as follows:

$$F_{Mg,\ carb} = E_a \times [Mg]_{carb,\ a} - E_b \times [Mg]_{carb,\ b} \quad (7)$$

Here, $[Mg]_{carb,\ a}$ = 0.37 mol·kg^{-1} corresponds to all Mg in carbonates (calcite and dolomite), and $[Mg]_{carb,\ b}$ = 0.04 mol·kg^{-1} corresponds to Mg only in calcite with a molar Mg/Ca ratio of 0.08 in the East China upper crust.

The reconstructed Mg release flux from weathering of silicate ($F_{Mg,\ sil}$) and carbonate ($F_{Mg,\ carb}$) related to the late Oligocene monsoon advance in East Asia shows that both fluxes account for their respective modern global flux 5-17% based on erosion flux variation reported by Clift et al. (2004) and ~1.5-17% based on erosion flux variation reported by Métivier et al. (1999) (Figs. 4b and 4c; the modern Mg flux from silicate weathering and carbonate weathering is 2-2.5×10^{12} mol·yr^{-1} and 2-2.2×10^{12} mol·yr^{-1}, respectively, according to Higgins and Schrag, 2015). The Mg oceanic cycle during the Cenozoic is characterized by a rise in the Mg content in the ocean (e.g., Horita et al., 2002). The rise in the sea water Mg concentration from 38 mmol·kg^{-1} at 37 Ma to 55.1 mmol·kg^{-1} at present (Horita et al., 2002) requires an average rate of increase of 0.46 mmol·Ma^{-1}. The combined Mg flux of silicate and carbonate weathering related to the late Oligocene monsoon advance in East Asia accounts for a rate of increase of the seawater Mg concentration is 0.18-0.45 mmol·Ma^{-1} based on erosion flux variation reported by Clift et al. (2004) and 0.05-0.46 mmol·Ma^{-1} based on erosion flux variation reported by Métivier et al. (1999) since the late Oligocene. Our results clearly suggest that at least a significant portion of this rise in seawater Mg content corresponds to the weathering of Mg-silicates and dolomite-rich carbonates in East China rather than just changes in the amount of Mg removed from seawater (Higgins and Schrag, 2015).

4.3 Carbon consumption flux linked to the monsoon advance

Similar to the Mg flux estimation, the flux of long-term CO_2 consumption by silicate weathering linked to the monsoon advance, F_{sil}, can be calculated as follows:

$$F_{sil} = E_a \times C_{sil,\ a} - E_b \times C_{sil,\ b} \quad (8),$$

where $C_{sil,\ a}$ is 1.04 mol·kg^{-1}, which is the mean of C_{sil} values for SCS sediments and red soils in subtropical China (Fig. 3); and $C_{sil,\ b}$ is 0.43 mol·kg^{-1}, identical to XF loess.

The reconstructed fluxes of long-term CO_2 consumption by silicate weathering (F_{sil}) (Fig. 4e) account for 3-8% of modern global flux of continental rock weathering (8.7×10^{12} mol·yr^{-1}, Gaillardet et al. 1999) based on the erosion flux variation by Clift et al. (2004) and ~1-9% by Métivier et al. (1999). It should be noted that 98% of our estimated F_{sil} is attributed to Ca-Mg-silicate weathering since (ΔMg_0+ΔCa_0) accounts for ~80% C_{sil} of all samples (Fig. 3a). The modern estimate of CO_2 consumption

fluxes by Ca-Mg silicate is 5×10^{12} mol·yr^{-1} (Gaillardet et al. 1999), which is ~60% of the modern global flux of continental rock weathering. Thus, if only Ca-Mg-silicate weathering is considered, our estimated flux regarding weathering of Ca-Mg silicate accounts for modern global flux of continental Ca-Mg-silicate weathering was 5-13% based on the given erosion flux variation reported by Clift et al. (2004) and ~1-16% based on the erosion flux variation reported by Métivier et al. (1999).

In the same way, the flux of organic carbon burial linked to the monsoon advance, F_{oc}, could be calculated as follows:

$$F_{oc}=E_a\times M_a\cdot\times f_a-E_b\times M_b\times f_b \quad (9),$$

The reconstructed organic carbon burial flux (F_{oc}) shows <3.5% of the modern global flux of organic carbon for both erosion rate models (Fig. 4f). This organic carbon burial flux is approximately 25% of the contemporary CO_2 consumption by silicate weathering (Fig. 4f), which also contrasts with the Himalayas, where the organic carbon burial flux is much larger than that of silicate weathering (France-Lanord and Derry, 1997).

The reconstructed long-term CO_2 consumption fluxes by silicate weathering and organic burial temporally vary, but the total amount ($F_{sil}+F_{oc}$) is within the same order as that in the Himalayas (1.28×10^{12} mol·yr^{-1}; France-Lanord and Derry, 1997). If the Cenozoic long-term silicate weathering fluxes are relatively stable (Caves et al., 2016), our reconstructed long-term CO_2 consumption fluxes by silicate weathering and organic burial can induce an imbalance in the geological carbon cycle. For long-term CO_2 consumption fluxes by silicate weathering, weathering of Mg silicate (ΔMg) accounts for 64-72% of total CO_2 consumption (Δ_{sil}), with a mean of ~69% (Table S3). Considering that the study region occupies ~2% of the total continental area, our study suggests a significant additional atmospheric CO_2 sink by silicate weathering when Mg-bearing minerals are subjected to weathering in response to this climatic reorganization since the late Oligocene. Such intensification of the weathering of the Yangtze and North China cratons will also contribute to the required increasing land surface reactivity during the Neogene (e.g., Kump and Arthur 1997; Caves et al. 2016; Caves Rugenstein et al., 2019). Additionally, fast and congruent weathering of dolomite-rich carbonate minerals (~10%) in the upper crust of humid subtropical China after the monsoon advance may also contribute a long-term carbon sink by aquatic photosynthesis (e.g., Liu et al., 2018).

5 Implications for tectonic-climatic linkage

Our modelling results show a significant increase in annual precipitation, with

magnitudes of ~100->400 mm, in response to topographic changes in the northern TP (Fig. 7). Moreover, most of the annual precipitation increase occurred in summer, especially over a large part of the Yangtze and North China cratons (Fig. 5), which indicates that the East Asian monsoon climate system might have been established or greatly strengthened. In summer, topographically elevated heating leads to strengthening of the low over Asia, with which the anomalous southeasterly and/or southwesterly winds mainly occur over East China (Fig. 5d). Thus, the modelling results indicate that the East Asian summer monsoon circulation has been established or is greatly stronger than it previously was. This strongly suggests that a tectonic-climatic linkage induced by the uplift of the northern TP has played a major role in the establishment of East Asian monsoon cycles in East China (e.g., Tada et al., 2016). The rapid late Oligocene-early Miocene uplift of the TP and a series of concomitant tectonic events are evidenced by various studies of tectonic deformation and volcanic rock emplacement (Lu et al., 2018). The size of the India-Asia collision thus had a prominent effect on the reorganization of the climatic patterns beyond the collision zone with the northward advance of the East Asian monsoon in tectonically inactive subtropical China, which, in turn, induced a globally significant silicate weathering CO_2 sink.

The study of orogenic effects on the global climate during the Cenozoic has focused almost exclusively on the India-Asia collision zone (e.g., Raymo and Ruddiman, 1992; France-Lanord and Derry, 1997). Our study suggests that the significant rise in CO_2 consumption induced by climatic changes and enhanced erosion in both South and East Asia is an effect of the Indian-Asian collision and uplift of the TP. This effect is characterized by an approximately equal order of magnitude between the direct effect of the orogeny via enhanced carbon burial in South Asia and the indirect effect that enhanced the weathering of Mg-rich silicate of the Yangtze craton and surrounding terrane. The unusual nature of the exposed crust in East China suggests that the tectonic impact on Cenozoic cooling via modulation of the geological carbon cycle is particularly intense, and such forcing might not be fully extrapolated to older global-scale orogeny. Our study thus illustrates how complex perturbations of global climate and atmospheric CO_2 levels by orogenic uplift can be and how important the nature of the crust is not only involved in collisions but also around collisions. This last point might have generated an imbalance in the global carbon cycle since it is not involved in any tectonic feedback but is sensitive to climate feedback, which may have contributed to the sharp atmospheric CO_2 decline during the late Oligocene and early Miocene transition (e.g., Beerling and Royer, 2011) and land reactivity that even regulates Neogene global cooling (Caves

Rugenstein et al. et al., 2019). Although there are many unresolvable uncertainties, e.g., erosion fluctuations over short and long timescales (Métivier and Gaudemer, 1999; Clift et al., 2006), our study has provided a first-order estimate of the global geochemical cycle regarding carbon and magnesium linked to such complex tectonic-climate linkages.

Acknowledgements

This study was co-supported by the Second Tibetan Plateau Scientific Expedition and Research (STEP) program (Grant No: 2019QZKK0707), the Strategic Priority Research Program of the Chinese Academy of Sciences (Grant No: XDA20070201), the National Natural Science Foundation of China (Grant Nos., 41771236, 41620104002) and the Basic Science Center for Tibetan Plateau Earth System (CTPES, 41988101-01). Y. Yang is supported by the Youth Innovation Promotion Association (2018095) of the Chinese Academy of Sciences. The model simulations were performed on TianHe-2, thanks for the support of National Supercomputer Center in Guangzhou (NSCC-GZ).

Conflict of interest: The authors declare that they have no conflict of interest.

References

Beerling DJ, Royer DL. Convergent Cenozoic CO_2 history. Nat Geosci 2011;4:418-420.

Blair NE, Aller RC. The Fate of Terrestrial Organic Carbon in the Marine Environment. Ann Rev Mar 2012;4:401-423.

Blum JD, Gazis CA, Jacobson AD, et al. Carbonate versus silicate weathering in the Raikhot watershed within the High Himalayan Crystalline Series. Geology 1998;26:411-414.

Caves JK, Jost AB, Lau KV, et al. Cenozoic carbon cycle imbalances and a variable silicate weathering feedback. Earth Planet Sc Lett 2016;450:152-163.

Caves Rugenstein JK, Ibarra D, von Blanckenburg F. Neogene cooling driven by land surface reactivity rather than increased weathering fluxes. Nature 2019;571:99-102.

Chappell J, Zheng H, Fifield K. Yangtse River sediments and erosion rates from source to sink traced with cosmogenic 10Be: Sediments from major rivers. Palaeogeogr Palaeoclimat Palaeoecol 2006;241:0-94.

Clift PD, Layne GD, Blusztajn J. Marine sedimentary evidence for monsoon

492 strengthening, Tibetan uplift and drainage evolution in East Asia. In: Clift P, Wang P,
493 Kuhnt W, Hayes DE, editors. Continent-Ocean Interactions within the East Asian
494 Marginal Seas. 2004, p. 255-282.
495 Clift PD. Controls on the erosion of Cenozoic Asia and the flux of clastic
496 sediment to the ocean. Earth Planet Sci Lett 2006;241:571-580.
497 CNEMC (China National Environmental Monitoring Centre). Background Values
498 of Elements in Soils of China. Beijing: China Environmental Science Press; 1990.
499 France-Lanord C, Derry LA. Organic carbon burial forcing of the carbon cycle
500 from Himalayan erosion. Earth Planet Sci Lett 1997;390:65-67.
501 Gaillardet J, Dupré B, Louvat P, et al. Global silicate weathering and CO_2
502 consumption rates deduced from the chemistry of large rivers. Chem Geol
503 1999;159:0-30.
504 Gaillardet J, Galy A. Himalaya-carbon sink or source? Science
505 2008;320:1727-1728.
506 Galy V, France-Lanord C, Beyssac O, et al. Efficient organic carbon burial in the
507 Bengal fan sustained by the Himalayan erosional system. Nature 2007;450:407-410.
508 Galy V, Peucker-Ehrenbrink B, Eglinton T. Global carbon export from the
509 terrestrial biosphere controlled by erosion. Nature 2015;521:204-207.
510 Gao S, Zhang B, Xie Q, et al. Average chemical compositions of post-Archean
511 sedimentary and volcanic rocks from the Qinling Orogenic Belt and its adjacent North
512 China and Yangtze Cratons. Chem Geol 1991;92:261-282.
513 Gao S, Luo T, Zhang B, et al. Chemical composition of the continental crust as
514 revealed by studies in East China. Geochim Cosmochim Acta 1998;62:1959-1975.
515 Guo Z, Sun B, Zhang Z, et al. A major reorganization of Asian climate by the
516 early Miocene. Clim Past 2008;4:153-174.
517 He M, Zheng H, Clift PD, et al. Geochemistry of fine-grained sediments in the
518 Yangtze River and the implications for provenance and chemical weathering in East
519 Asia. Prog Earth Planet Sci 2015;2:32.
520 He Z, Zhang M, Wilson MJ. Distribution and classification of red soils in China.
521 In: Wilson MJ, He Z, Yang X, editors. The red soils of China. Springer Netherlands;
522 2004, p. 29-33.
523 Hilton RG, Galy A, Hovius N, et al. Efficient transport of fossil organic carbon to
524 the ocean by steep mountain rivers: An orogenic carbon sequestration mechanism.
525 Geology 2011;39:71-74.
526 Higgins JA, Schrag DP. The Mg isotopic composition of Cenozoic
527 seawater-evidence for a link between Mg-clays, seawater Mg/Ca, and climate. Earth
528 Planet Sci Lett 2015;416:73-81.

Lin J, Dai J, Zhuang G, et al. Late Eocene-Oligocene High Relief Paleotopography in the North Central Tibetan Plateau: Insights From Detrital Zircon U-Pb Geochronology and Leaf Wax Hydrogen Isotope Studies. Tectonics 2020;39: e2019TC005815.

Hong H, Wang C, Zeng K, et al. Geochemical constraints on provenance of the mid-Pleistocene red earth sediments in subtropical China. Sediment Geol 2013;290:97-108.

Horita J, Zimmermann H, Holland HD. Chemical evolution of seawater during the Phanerozoic: Implications from the record of marine evaporites. Geochim Cosmochim Acta 2002;66:733-3756,

Kump LR, Arthur MA. In: Ruddiman WF, editor. Tectonic Uplift and Climate Change. Plenum Press; 1997, p. 399-426.

Kump LR, Brantley SL, Arthur MA. Chemical weathering, atmospheric CO_2, and climate. Annu Rev Earth Planet Sci Lett 2000;28:611-667.

Lee H, Galy V, Feng X, et al. Sustained wood burial in the Bengal Fan over the last 19 My. Proc Natl Acad Sci USA 2019;116:22518-22525.

Liang M, Guo Z, Kahmann AJ, et al. Geochemical characteristics of the Miocene eolian deposits in China: Their provenance and climate implications. Geochem Geophys Geosyst 2009;10:Q04004.

Licht A, Van Cappelle M, Abels HA, et al. Asian monsoons in a late Eocene greenhouse world. Nature 2014;513:501-506.

Liu X, Sun H, Miao Y, et al. Impacts of uplift of northern Tibetan Plateau and formation of Asian inland deserts on regional climate and environment. Quat Sci Rev 2015;116:1-14.

Liu Z, Trentesaux A, Clemens SC, et al. Clay mineral assemblages in the northern South China Sea: implications for East Asian monsoon evolution over the past 2 million years. Mar Geol 2003;201:133-146.

Liu Z, Macpherson G, Groves G, et al. Large and active CO_2 uptake by coupled carbonate weathering. Earth-Sci Rev 2018;182;42-49.

Lu H, Tian X, Yun K, et al. Convective removal of the Tibetan Plateau mantle lithosphere by ~26 Ma. Tectonophysics 2018;731:17-34.

Métivier F, Gaudemer Y. Stability of output fluxes of large rivers in South and East Asia during the last 2 million years: implications on floodplain processes. Basin Res 1999;11:293-303.

Miao Y, Wu F, Herrmann M, et al. Late early Oligocene East Asian summer monsoon in the NE Tibetan Plateau: Evidence from a palynological record from the Lanzhou Basin, China. J Asian Earth Sci 2013;75:46-57.

566 Milliman JD, Syvitski PM. Geomorphic/tectonic control of sediment discharge to
567 the ocean: the importance of small mountainous rivers. J Geol 1992;100:525-544.
568 Raymo ME, Ruddiman WF. Tectonic forcing of late Cenozoic climate. Nature
569 1992;359:117-122.
570 Rudnick RL, Gao S. Composition of the continental crust. Treatise on
571 Geochemistry 2004;3:1-65.
572 Shipboard Scientic Party, Site 1146. In: Wang P, Prell WL, Blum P, et al. editors.
573 Proc ODP Init Rep; 2000, 184.
574 Song B, Spicer RA, Zhang K, et al. Qaidam Basin leaf fossils show northeastern
575 Tibet was high, wet and cool in the early Oligocene. Earth Planet Sci Lett
576 2020;537:116175.
577 Spicer RA., Yang J, Herman AB, et al. Asian Eocene monsoons as revealed by
578 leaf architectural signatures. Earth Planet Sci Lett 2020;449: 61-68.
579 Sun X, Wang P. How old is the Asian monsoon system? — Palaeobotanical
580 records from China. Journal of Tongji University, 2005;222:181-222.
581 Tada R, Zheng H, Clift PD. Evolution and variability of the Asian monsoon and
582 its potential linkage with uplift of the Himalaya and Tibetan Plateau. Prog Earth
583 Planet Sci 2016;3:4.
584 Tapponnier P, Xu ZQ, Roger F, et al. Oblique stepwise rise and growth of the
585 Tibet Plateau. Science 2001;294:1671-1677.
586 Wan S, Clift PD, Li A, et al. Geochemical records in the South China Sea:
587 implications for East Asian summer monsoon evolution over the last 20 Ma.
588 Geological Society of London, Special Publications. 2010;342:245-263.
589 Wieder WR, Boehnert J, Bonan GB, Langseth M. Regridded Harmonized World
590 Soil Database v1.2. Data set. Available on-line [http://daac.ornl.gov] from Oak Ridge
591 National Laboratory Distributed Active Archive Center, Oak Ridge, Tennessee, USA;
592 2014.
593 Xie Y, Wu F, Fang X. A major environmental shift by the middle Eocene in
594 southern China: Evidence from palynological records. Rev Palaeobot Palynol
595 2020;104226.
596 Zhang J, Liu Y, Fang X, et al. Large dry-humid fluctuations in Asia during the
597 Late Cretaceous due to orbital forcing: A modeling study. Palaeogeogr Palaeoclimat
598 Palaeoecol 2019;533:109230.
599 Zhang J, Lu J, Xing X, et al. Element geochemistry of laterite in the Dongting
600 Lake area, Hunan, China and its indicative significance. Geol Bull China 2007;
601 26:1435-1444.
602 Zhang R, Jiang D, Zhang Z, et al. Comparison of the climate effects of surface

603 uplifts from the northern Tibetan Plateau, the Tianshan, and the Mongolian Plateau on
604 the East Asian climate. J Geophys Res-Atmos 2017;122: 7949-7970.
605 Zheng Y, Xiao W, Zhao G. Introduction to tectonics of China. Gondwana Res
606 2013; 23:1189–1206.
607

608 **Figures captions**

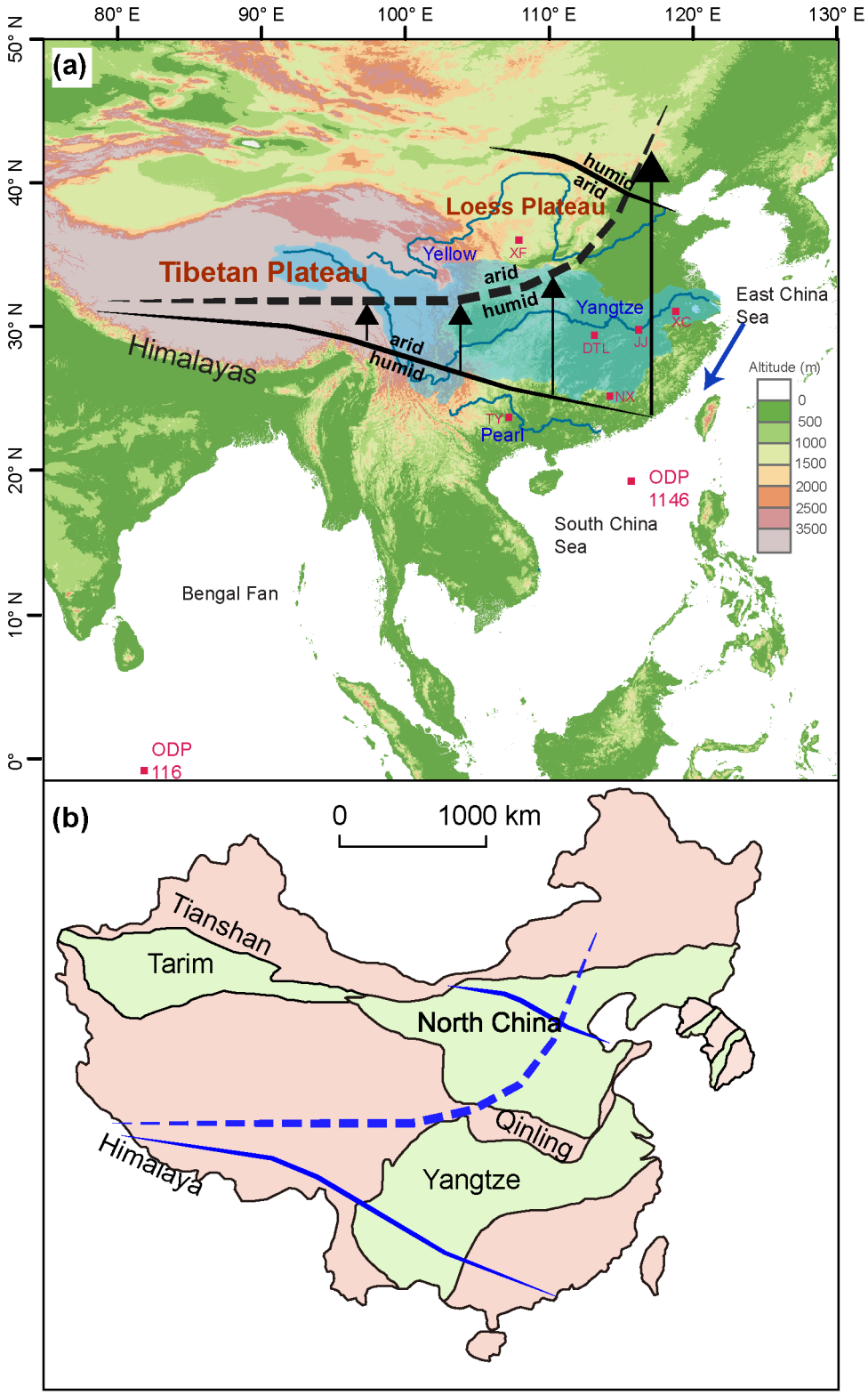

609

610 **Figure 1 (a)** Cenozoic humid/arid boundaries in China for the Palaeogene (black bold
611 line) and the Neogene to Quaternary (black dashed line). Black arrows show the
612 northward migration of the humid zone. Red squares are locations of the studied soils
613 (XF, Xifeng loess; DTL, Dongting Lake, JJ, Jiujiang; XC, Xuancheng; NX, Nanxiong;

and TY, Tianyang) and sediments (ODP site 1146 in the South China Sea, SCS; ODP site 116 in the Bengal Fan). The light blue shaded area marks the drainage area of the Yangtze River. The blue arrow shows the modern transport path of sediments from the Yangtze River mouth to the SCS (Liu et al., 2003). **(b)** Simplified tectonic map of the Chinese continent showing the distributions of major cratons (green area) and orogens (light brown area) (redrawn from Gao et al., 1998 and Zheng et al., 2013). Black lines mark major faults. The northward migration of the humid zone (the area between the blue bold and dashed lines) impacted the majority of the Yangtze craton.

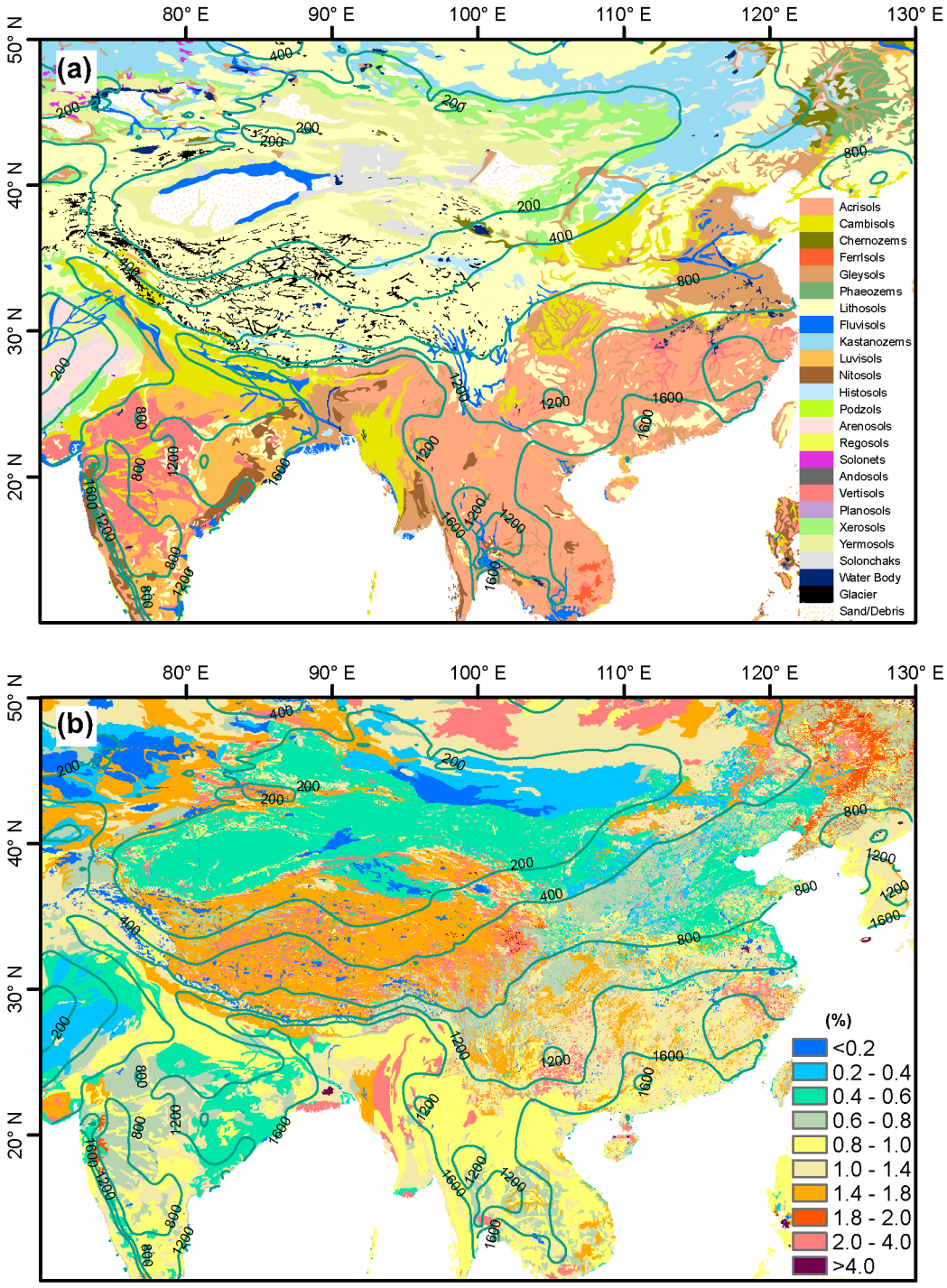

Figure 2 (a) Modern soil type distributions with isohyets (mm) in Asia. Soil type data are based on the FAO-UNESCO Soil Map of the World (http://www.fao.org/geonetwork/srv/en/main.home). **(b)** Soil organic carbon content (%) distributions with isohyets (mm) in China. Organic carbon data refer to surface soil horizons (0 to 30 cm) from Wieder et al. (2014). Isohyet data are from updated high-resolution grids of monthly climatic observations acquired from the CRU TS

v3.24 dataset (http://www.cru.uea.ac.uk/).

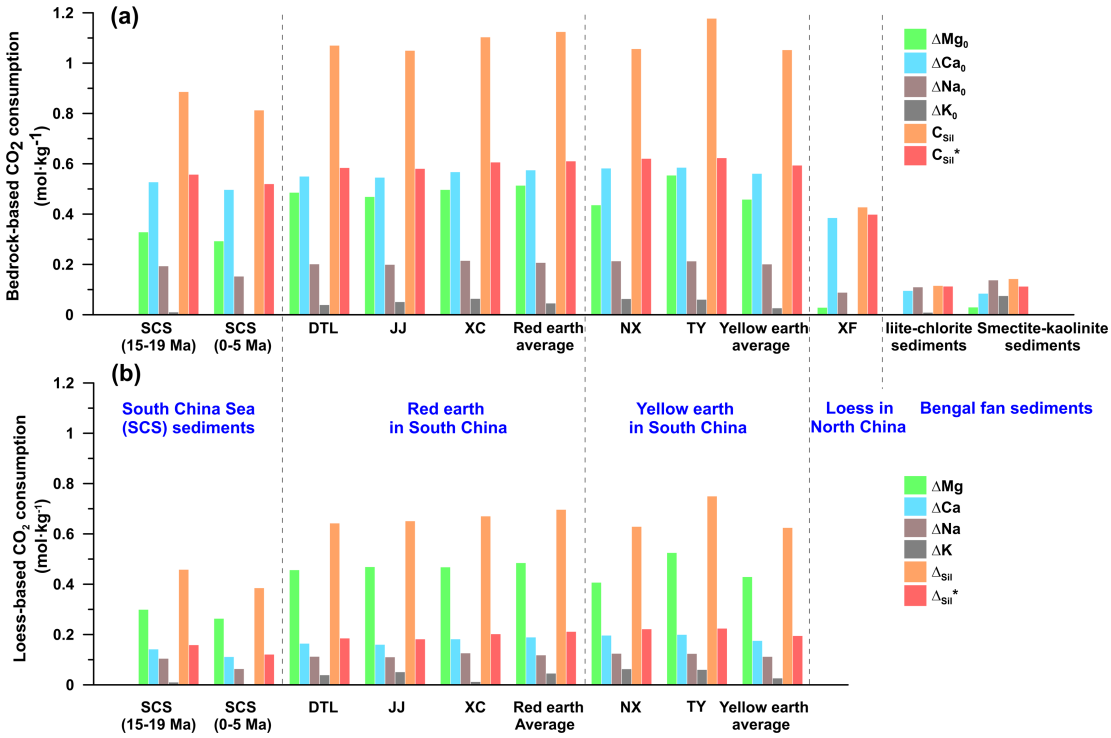

Figure 3 (a) Consumption of atmospheric CO_2 by silicate weathering estimated from the difference between the chemistry of various sediments and bedrock. The Bengal Fan sediment composite is based on unaltered Himalayan source rocks (France-Lanord and Derry, 1997); others are calculated based on the carbonate-free upper crust of East China (Gao et al., 1998). (**b**) Difference in atmospheric CO_2 consumption by silicate weathering between various sediments used for the post-late Oligocene monsoon-influenced region (sediments in the South China Sea (SCS)/various soils in South China) and loess from Northwest China.

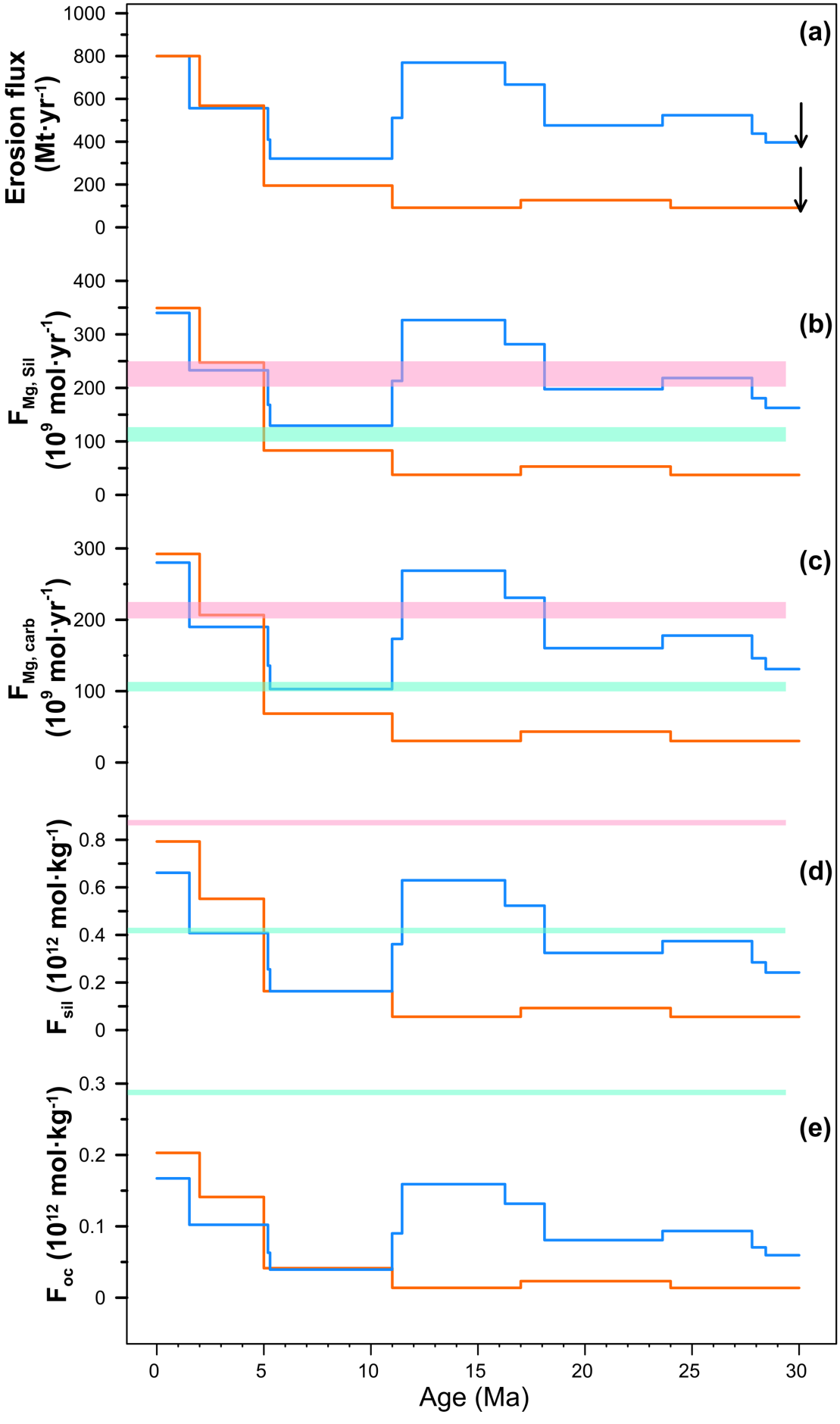
(a)
Erosion flux
(Mt·yr-1)
1000
800
600
400
200
0
(b)
F Mg, Sil
(10 9 mol·yr-1)
400
300
200
100
0
(c)
F Mg, carb
(10 9 mol·yr-1)
300
200
100
0
(d)
F sil (10 12 mol·kg-1)
0.8
0.6
0.4
0.2
0
(e)
F oc (10 12 mol·kg-1)
0.3
0.2
0.1
0
0
5
10
15
20
25
30
Age (Ma)

639

Figure 4 The estimated erosion flux **(a)**, CO_2 consumption flux **(b)**, and Mg release fluxes from weathering of silicate ($F_{Mg, sil}$) **(c)** and carbonate ($F_{Mg, carb}$) **(d)** as well as organic burial flux **(e(,** related to late Oligocene monsoon advance in East Asia. The orange and blue cruves in **(a-e)** are based on two reconstructed sediment discharge fluxes based on the East China Platform dataset (Métivier et al., 1999) and integrative flux of the Pearl River and East China Sea basins (Clift et al., 2004), respectively. Curves in **(b)** were reconstructed by our estimated modern physical erosion flux of ~800×10^6 $t\cdot yr^{-1}$ for the monsoon-influenced region by multiplying the relative variations of two sediment discharge models. The black arrows in **(b)** mark the erosion flux before the late Oligocene climatic reorganization. The pink and green shaded areas in (**b-e**) mark the 10% and 5% levels of the modern flux for each panel, respectively.

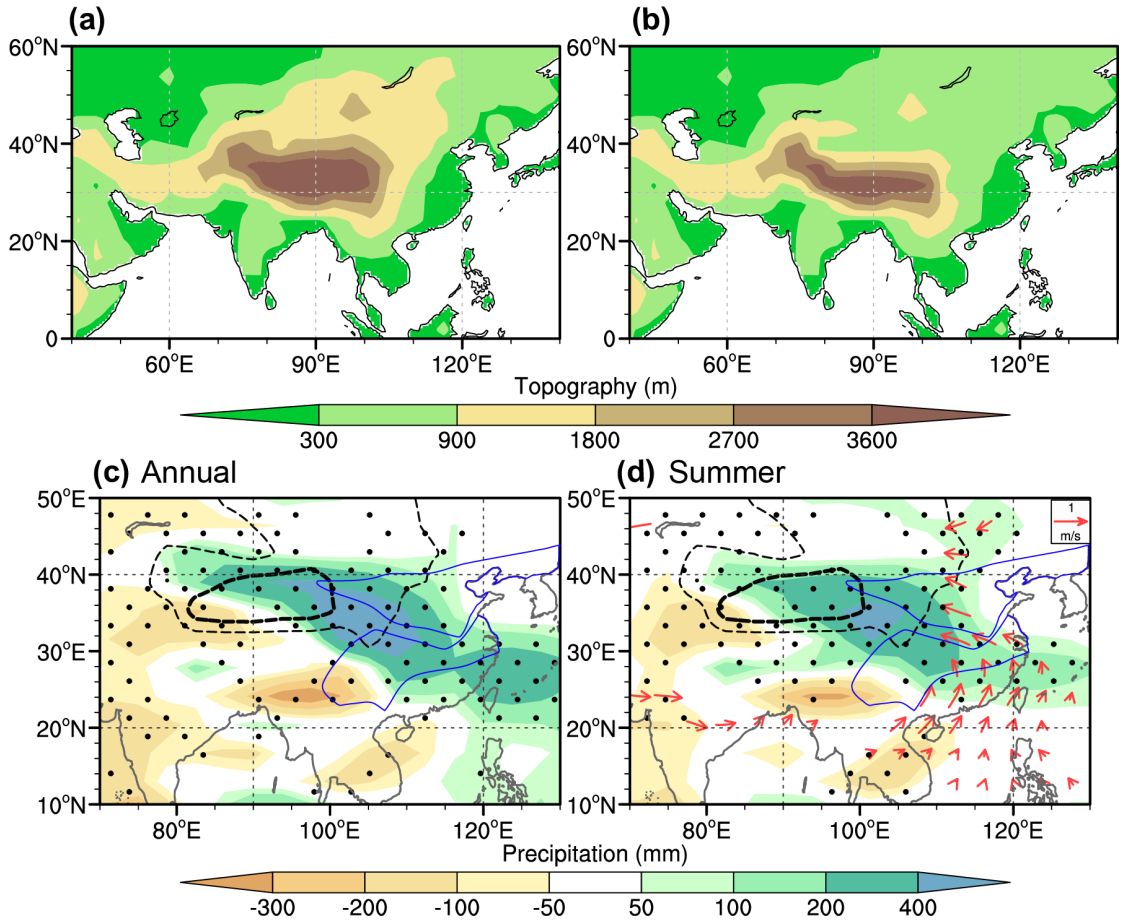

Figure 5 Modern topography **(a)** and removal of the northern Tibetan Plateau **(b)** over Asia. Differences in **(c)** annual precipitation (coloured areas) and **(d)** summer monsoon (May to September) precipitation (coloured areas) and 850 hPa winds (red arrows) between the climate model experiments with the modern topography. Dotted areas correspond to places with confidence levels greater than 95% (using Student's

659 *t*-test) in precipitation change. The thick and thin black dashed lines mark the contour
660 lines of 500 and 1500 m for topography removal, respectively, of the northern Tibetan
661 Plateau between the two climate models. The blue lines indicate the contours of the
662 Yangtze and North China cratons.